

Multislip Friction with a Single Ion

Ian Counts,¹ Dorian Gangloff,^{1,2} Alexei Bylinskii,^{1,3} Joonseok Hur,¹ Rajibul Islam,^{1,4} and Vladan Vuletić^{1,*}

¹*Department of Physics and Research Laboratory of Electronics, Massachusetts Institute of Technology, Cambridge, Massachusetts 02139, USA*

²*Cavendish Laboratory, JJ Thompson Ave, Cambridge CB3 0HE, United Kingdom*

³*Department of Chemistry and Chemical Biology and Department of Physics, Harvard University, Cambridge, Massachusetts 02138, USA*

⁴*Institute for Quantum Computing and Department of Physics and Astronomy, University of Waterloo, Waterloo, Ontario N2L 3G1, Canada*

(Received 1 May 2017; published 24 July 2017)

A trapped ion transported along a periodic potential is studied as a paradigmatic nanocontact frictional interface. The combination of the periodic corrugation potential and a harmonic trapping potential creates a one-dimensional energy landscape with multiple local minima, corresponding to multistable stick-slip friction. We measure the probabilities of slipping to the various minima for various corrugations and transport velocities. The observed probabilities show that the multislip regime can be reached dynamically at smaller corrugations than would be possible statically, and can be described by an equilibrium Boltzmann model. While a clear microscopic signature of multislip behavior is observed for the ion motion, the frictional force and dissipation are only weakly affected by the transition to multistable potentials.

DOI: 10.1103/PhysRevLett.119.043601

Stick-slip friction is a ubiquitous nonequilibrium dynamical process that occurs at the interface between surfaces across a wide range of length scales [1–6]. The term stick slip describes the system’s response to an applied shear force: the surfaces slip out of a local minimum in the interface energy landscape, and stick into a new lower-energy minimum, releasing heat in the process.

Recent advances in atomic force microscopy (AFM) have extended the study of stick-slip friction to the atomic scale, where atom-by-atom slips occur at the interface between a probe tip and a periodic substrate [7–18]. For a single-atom probe, the number of local minima in the probe-substrate interaction potential is determined by the ratio of the periodic substrate potential to the spring constant with which the probe is bound to its support object. As the load on the probe is increased, or equivalently, the periodic substrate potential is deepened, the system transitions from a bistable regime (where the probe deterministically single slips from the first minimum to the second) to a multistable regime (where a probe can stochastically multislip to one of several local minima). This has been demonstrated in AFM simulations [19–22] and experiments [23–25] where single-slip and multislip events have been clearly differentiated. However, in the absence of control over dissipation rates and the microscopic energy landscape, it is difficult to tie the observations to *ab initio* friction models.

Following theoretical proposals [26–29], we have recently demonstrated a trapped-ion friction emulator with extensive control over all microscopic interface parameters [30–32]. In analogy to AFM, the emulator features a small probe (one or several trapped ions) transported over a

periodic substrate potential created by an optical standing wave [Figs. 1(a) and 1(b)] [33–35]. To date, we have used the emulator to study the velocity dependence of nano-friction [30], as well as the interplay between superlubricity [31,36–39] and the Aubry transition [32]. These studies and a recent study of zigzag ion chains [40] have focused on the single-slip regime.

In this Letter, we study multislip friction in deep substrate potentials. We observe the ion fluorescence associated with slip events, from which we directly extract the temperature- and velocity-dependent probabilities for the ion to localize in one of the available local minima. We find that at finite rethermalization times following a slip, the multislip regime can be reached dynamically at smaller corrugations than would be possible statically. We also find that the probabilities agree well with a simple Boltzmann model, despite the dynamical nature of the process. Remarkably, the average frictional energy dissipation U_{diss} and the maximal static friction force F_{static} are mostly unaffected by the transition from the single-slip to the multislip regime, increasing approximately linearly with the depth of the substrate potential.

The potential energy landscape experienced by the ion is produced by the combination of an electrostatic harmonic potential provided by a linear Paul trap [41] and a sinusoidal optical lattice [30–32,35]. The potential energy of the ion at position x is given by the Prandtl-Tomlinson model [42,43],

$$\frac{V(x)}{Ka^2} = \frac{1}{2} \left(\frac{x - x_0}{a} \right)^2 + \frac{\eta}{4\pi^2} \left[1 - \cos \left(\frac{2\pi x}{a} \right) \right]. \quad (1)$$

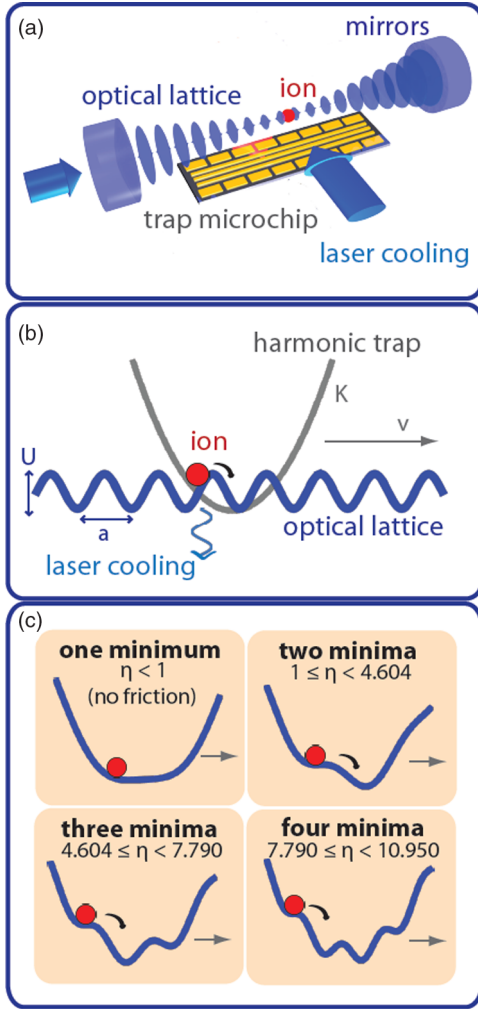


FIG. 1. (a) Schematic of the experimental setup. A $^{174}\text{Yb}^+$ ion is trapped by a linear Paul trap, located $135\ \mu\text{m}$ above the surface of a lithographic microchip. The chip generates radial trapping with a rf field and axial trapping with a dc harmonic potential. An axial optical-lattice standing wave is produced by 370 nm light, blue detuned from the $^2S_{1/2} \rightarrow ^2P_{1/2}$ atomic transition by 12.6 GHz. Ion fluorescence is collected during laser cooling. (b) Stick-slip friction in a periodic optical potential. As the harmonic trap is translated at speed v , it drags the ion along the sinusoidal optical-lattice potential, causing the ion to slip. The excess energy acquired during a slip is dissipated by continuous laser cooling. (c) Combined harmonic-sinusoidal potential for different values of the corrugation parameter η . The potential energy landscape is drawn just before the slipping point, where the leftmost minimum vanishes and a potential with initially n local minima has $n - 1$ available minima to which the ion can slip. Note that for $n = 1$, there is no energy barrier and, consequently, no stick-slip friction.

The first term is attributed to the harmonic trap at position x_0 , corresponding to a spring with constant $K = m\omega_0^2$ [m is the mass of the $^{174}\text{Yb}^+$ ion and $\omega_0/(2\pi) \approx 360$ kHz is the axial vibrational frequency of the harmonic trap]. The second term is due to the ac Stark shift of the lattice with period

$a = 185\ \text{nm}$ [31]. The number of local minima in $V(x)$ is determined by the corrugation parameter $\eta = (\omega_L/\omega_0)^2$, with ω_L being the vibrational frequency at the lattice minima. By adjusting the optical-lattice amplitude to a maximum of $U/h = 40$ MHz, we change $\omega_L = \sqrt{2\pi^2 U/ma^2}$ up to $2\pi \times 1.1$ MHz, and thus tune η in the range $0 \leq \eta \leq 10$. Values of interest include $\eta = 1$, 4.604, and 7.790, which mark the transition to potentials with $n = 2$, $n = 3$, and $n = 4$ local minima, respectively [Fig. 1(c)].

The ion is transported by adjusting the potentials of the trap electrodes so as to translate the harmonic-trap position x_0 . Thus, we drive the ion over the optical lattice at constant average velocity $v = dx_0/dt$, forcing the ion to slip over lattice maxima [Fig. 1(c)]. During the transport, the ion is continuously laser cooled via Raman sideband cooling to a typical temperature of $50\ \mu\text{K}$ ($k_B T/U$ in the range 0.5 to 0.03 for η in the range 0.5 to 10) [35], and observed via the fluorescence emitted during the cooling process. For a stationary ion, the fluorescence peaks when its stable minimum becomes an inflection point, the moment when the ion is closest to the maximum of the optical-lattice potential [35]. After the ion slips over a lattice maximum, its fluorescence falls exponentially while it cools and localizes into a new local minimum.

Initializing the ion in the global potential minimum, and then transporting through consecutive slip events, we observe a series of fluorescence peaks; the relative heights of these peaks differentiate single-slip from multislip behavior. For an ion undergoing single slips, a series of equally spaced fluorescence peaks of equal height is observed, as the ion always localizes in the adjacent minimum after every slip event [Fig. 2(a)]. The transition to the multislip regime manifests itself as fluorescence peaks of different heights, associated with random localizations in more distant minima [Figs. 2(b) and 2(c)].

To see why the two slip modes result in different peak height distributions, we note that the fluorescence traces are averaged over multiple repetitions of the initialization-transport experiment. The more likely an ion is to slip at a particular time, the higher the associated averaged fluorescence peak. The ion is initialized in the global potential minimum; when this minimum vanishes due to trap translation, the ion always slips and fluoresces. Thus, the first peak f_1 is the largest. After this initial slip, if the ion localizes in the adjacent minimum (single slip), then further trap translation by one lattice period a causes the ion to slip and fluoresce again, and we observe $f_2 = f_1$. If it localizes instead in the next-adjacent minimum (multislip), then a fluorescence peak does not appear until translation by $2a$. A finite probability of next-adjacent localization results in a reduced peak $f_2 < f_1$ and a higher peak $f_3 > f_2$ [see Figs. 2(b) and 2(c)].

The relationship between the localization probabilities $\{p_A, p_B, p_C\}$ (where p_A denotes localization in the

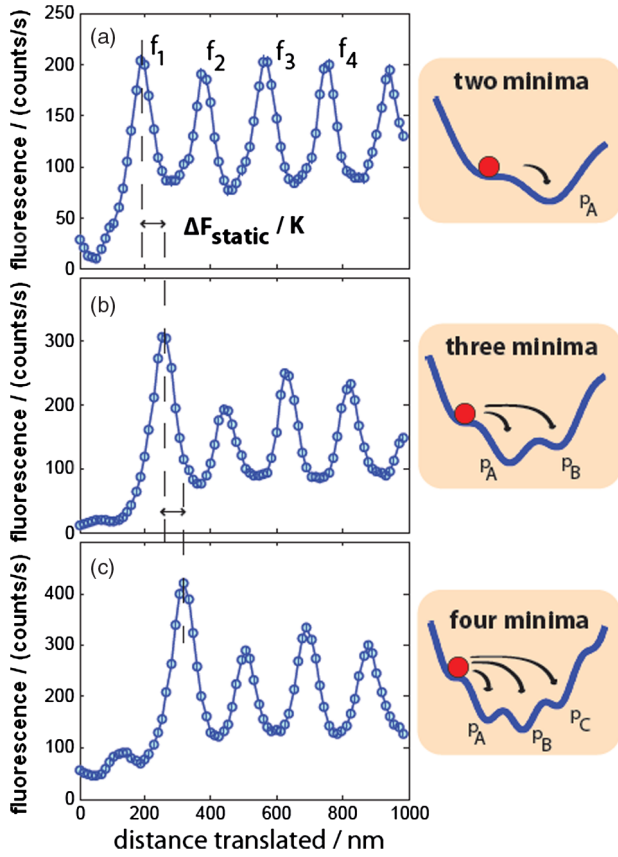


FIG. 2. Measured ion fluorescence as a function of trap translation, indicating single-slip vs multislip behavior. After the ion is prepared in the global energy minimum, the harmonic trap is translated at constant velocity across the optical standing wave. This forces the ion to slip over local potential maxima, resulting in fluorescence peaks. The fluorescence traces are averaged over an exposure time of 300 seconds, corresponding to roughly 1.5×10^5 realizations of the experiment. Error bars are statistical and indicate one standard deviation. (a) Fluorescence trace indicating single-slip behavior for a potential with $n = 2$ minima ($\eta = 3.2$). Fluorescence peaks are of equal height, indicating that the ion always slips to the adjacent minimum (lattice period $a = 185$ nm). There is a small variation of peak heights due to the finite recooling time (see the text). [(b) and (c)] Fluorescence traces indicating multislip behavior in a potential with $n = 3$ and $n = 4$ minima, respectively ($\eta = 6.4$ and $\eta = 9.6$). Fluorescence peaks vary in height, indicating that an ion can slip into one of multiple local minima, and therefore may not always slip when a given minimum disappears. Note the hysteretic delay of the peaks in these time traces compared to Fig. 2(a). This is due to the greater static friction force F_{static} exerted on the ion by the optical lattice at higher η . [See Ref. [31] and Fig. 4(a)].

adjacent minimum, p_B the next-adjacent minimum, etc.) and the peak height distribution $\{f_i\}$ is given by [44]

$$\begin{aligned} p_A &= f_2/f_1, \\ p_B &= -(f_2/f_1)^2 + f_3/f_1, \\ p_C &= (f_2/f_1)^3 - 2f_2f_3/f_1^2 + f_4/f_1. \end{aligned} \quad (2)$$

Note that the probability distribution is extracted directly from the observed peak heights without making assumptions about the localization process.

By measuring fluorescence patterns like the ones shown in Fig. 2 for different corrugation parameters η and transport velocities v , we extract localization probabilities over a range of experimental conditions (Fig. 3). For all three velocities shown, multislip behavior (second-next neighbor slip probability $p_B > 0$) is observed in the multistable regime ($\eta > 4.604$). This is a consequence of the underdamping of the system ($\gamma_c \ll \omega_0$), which guarantees that an ion, following a slip, can sample the full potential landscape before it recools at rate $\gamma_c = 10^4 \text{ s}^{-1}$ and localizes in a minimum. More surprising is the appearance of multislip events before the corrugation is deep enough to create multiple static minima (in the region of bistable potential $\eta < 4.604$, where a third minimum should not yet exist). This is the case for the two fastest transport speeds but not for the slowest transport. This can be readily explained by the change in the energy landscape during the recooling time γ_c^{-1} : by the time the ion is sufficiently cooled to localize, another potential minimum may have opened up if

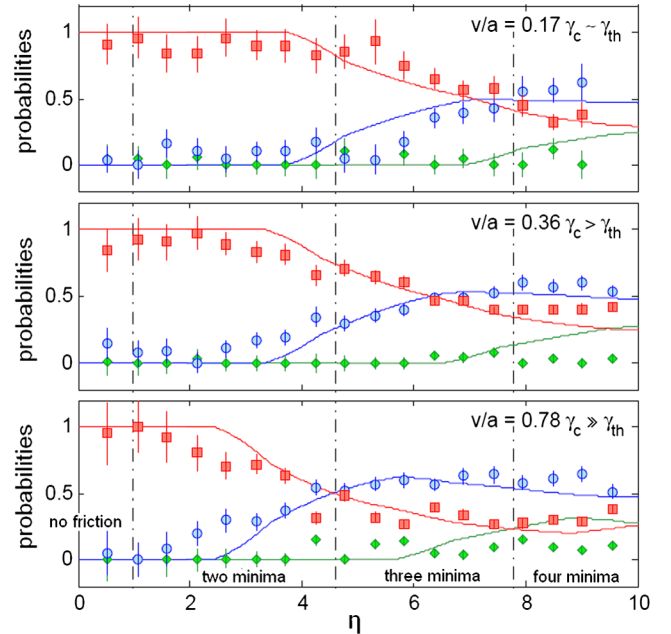


FIG. 3. Multislip probabilities vs corrugation parameter η for different transport velocities v . Data points are the extracted slipping probabilities p_A (slip to next minimum, red squares), p_B (slip to second-next minimum, blue circles), and p_C (slip to third minimum, green diamonds). Velocities are reported as functions of the system's recooling rate γ_c and thermal hopping rate γ_{th} , the rate at which the ion hops over a barrier due to its finite temperature (see the main text). Error bars are statistical and indicate one standard deviation. The multislip regime is distinguished by non-negligible values of p_B . Curves are calculated from a theoretical model. Vertical dash-dotted lines separate regimes with different numbers of minima [as in Fig. 1(c)].

$v/a \gtrsim \gamma_c$. Thus, we find that the multislip regime can be reached dynamically at smaller corrugations than would be possible statically.

The experimental data shown in Fig. 3 are overlaid with a theoretical model that takes into account the system's competing rates (transport rate v/a and recooling rate γ_c). Our model's central assumption is that an ion is more likely to localize in a lower-energy minimum and that this effect can be described by a quasiequilibrium Boltzmann probability $p_i \propto \exp(-[V_i(\tau)/k_B T(\tau)])$. Here, $V_i(\tau)$ is the potential energy of the i th minimum at time τ when the ion localizes, and $T(\tau)$ is the temperature of the ion at that time. To model its temperature, we note that an ion has some potential energy V_0 at the slipping point. This is converted into kinetic energy and dissipated exponentially by laser cooling: $k_B T(\tau) = V_0 \exp(-\gamma_c \tau)$. Our model's free parameter is the localization time, found to be $\tau = (65 \pm 5) \mu\text{s}$ by fitting the model to the data.

We note that the data set with the slowest transport speed is fitted with lower confidence by the model above $\eta > 4.604$. This discrepancy is the signature of another dynamical rate of the system, the thermal hopping rate $\gamma_{\text{th}} = 10^3 \text{ s}^{-1}$, observed previously in Refs. [30,45,46]. Thermal hopping across a barrier due to the ion's finite temperature dominates at the slowest transport speed, where $v/a \sim \gamma_{\text{th}}$ (the thermolubric regime [30]). Its effect on the fluorescence signal is to smooth the peak height distribution, which causes us to overestimate the value of p_A and underestimate p_B [44]. Evidently, the relationship between fluorescence and probability [Eq. (2)] is strictly valid only for faster transport speeds, where thermal hopping is negligible ($v/a \gg \gamma_{\text{th}}$).

Thermal hopping also affects the observed slip probability to the third minimum p_C , which for large η and large speed is distinctly smaller than predicted. The third minimum, most distant from the slipping point, has the smallest potential barrier and the longest dwell time before the minimum disappears, making the ion most susceptible to thermal hopping out of that minimum, even at fast transport speeds. Because a thermal hop at a random time does not result in an (averaged) fluorescence peak, we undervalue the localization probability p_C .

Figures 2 and 3 show clear delineations of single-slip and multislip behavior as a function of η . Interestingly, purely frictional quantities, like the maximal static friction force F_{static} and energy dissipated per slip U_{diss} , do not reveal clear signatures of the transition. Figure 4(a) shows that F_{static} exerted by the lattice on the ion increases monotonically with the corrugation parameter η , without any discernable changes near the critical values for multistability (F_{static} is determined from the observed hysteretic shift of the fluorescence peaks as a function of trap translation; see Fig. 2 and Ref. [31]). Figure 4(b) shows the calculated average energy U_{diss} dissipated per slip by laser cooling, determined from the measured slip

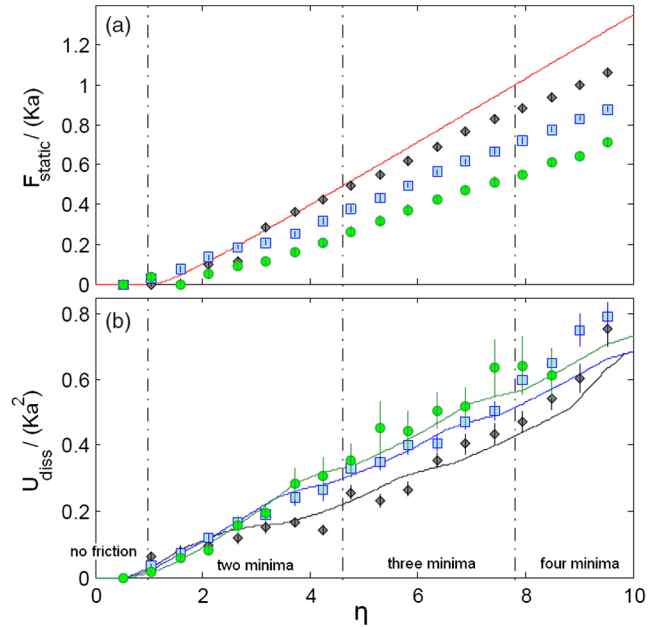


FIG. 4. (a) Measured static friction force vs η for three different drive velocities ($v/a = 0.17 \gamma_c$ for green circles, $v/a = 0.36 \gamma_c$ for blue squares, and $v/a = 0.78 \gamma_c$ for black diamonds). The velocity dependence of the slope is due to thermal hopping, which reduces friction for slow transport [30]. The red theory curve is a realization of the Prandtl-Tomlinson model with no free parameters, without thermal hopping. (b) Energy dissipated per slip vs η . Data points are calculated from experimentally determined values for p_i , while the curves use the model values for p_i from Fig. 3. Both use the calculated energy landscape. Vertical dash-dotted lines separate regimes with different numbers of minima.

probabilities p_i and the calculated energy landscape $V(t)$ [44]. Like F_{static} , the dissipated energy U_{diss} increases monotonically with the corrugation parameter η , and shows little dependence on the number n of potential minima in the energy landscape for $n \geq 2$. This can be attributed to the cancellation of two competing effects: if an ion slips to the second-next minimum rather than to the next minimum, it releases more heat, as the second-next minimum is lower in energy by the time the ion localizes. On the other hand, an ion slipping to a more distant minimum waits longer before it slips again. Thus, to leading order, the dissipation is independent of the slipping mode. To higher order, the slope $dU_{\text{diss}}/d\eta$ is slightly reduced for a potential with more minima, as the reduction in slip frequency overpowers the smaller increase in dissipated energy per slip. This trend is visible in Fig. 4(b), where the slope is reduced at the transition between single-slip and multislip behavior.

In this work, we have measured the slip probabilities for stick-slip friction in a multistable energy landscape, and have shown that the dynamic stick-slip process can be described by a quasiequilibrium model. We suggest that the model's predictive power could be used in nanopositioning applications: by tuning system parameters, a probe could be engineered to multislip to a specific potential minimum. In

the future, these studies could be extended to the quantum regime in order to study quantum annealing in a multistable energy landscape.

This work was supported in part by the NSF, the NSF CUA, and the MURI program through ONR.

*vuletic@mit.edu

- [1] C. H. Scholz, *Nature (London)* **391**, 37 (1998).
- [2] M. Urbakh, J. Klafter, D. Gourdon, and J. Israelachvili, *Nature (London)* **430**, 525 (2004).
- [3] V. Bormuth, V. Varga, J. Howard, and E. Schäffer, *Science* **325**, 870 (2009).
- [4] Y. Mo, K. T. Turner, and I. Szlufarska, *Nature (London)* **457**, 1116 (2009).
- [5] M. Urbakh and E. Meyer, *Nat. Mater.* **9**, 8 (2010).
- [6] A. Vanossi, N. Manini, M. Urbakh, S. Zapperi, and E. Tosatti, *Rev. Mod. Phys.* **85**, 529 (2013).
- [7] G. Binnig, C. F. Quate, and Ch. Gerber, *Phys. Rev. Lett.* **56**, 930 (1986).
- [8] R. W. Carpick and M. Salmeron, *Chem. Rev.* **97**, 1163 (1997).
- [9] E. Gnecco, R. Bennewitz, T. Gyalog, Ch. Loppacher, M. Bammerlin, E. Meyer, and H.-J. Güntherodt, *Phys. Rev. Lett.* **84**, 1172 (2000).
- [10] I. Szlufarska, M. Chandross, and R. W. Carpick, *J. Phys. D* **41**, 123001 (2008).
- [11] E. Riedo, E. Gnecco, R. Bennewitz, E. Meyer, and H. Brune, *Phys. Rev. Lett.* **91**, 084502 (2003).
- [12] X. Zhao, S. R. Phillpot, W. G. Sawyer, S. B. Sinnott, and S. S. Perry, *Phys. Rev. Lett.* **102**, 186102 (2009).
- [13] L. Jansen, H. Hölscher, H. Fuchs, and A. Schirmeisen, *Phys. Rev. Lett.* **104**, 256101 (2010).
- [14] I. Barel, M. Urbakh, L. Jansen, and A. Schirmeisen, *Phys. Rev. B* **84**, 115417 (2011).
- [15] S. Y. Krylov and J. W. M. Frenken, *Phys. Status Solidi (b)* **251**, 711 (2014).
- [16] E. Meyer and E. Gnecco, *Friction and wear in machinery* **2**, 106 (2014).
- [17] Q. Li, Y. Dong, D. Perez, A. Martini, and R. W. Carpick, *Phys. Rev. Lett.* **106**, 126101 (2011).
- [18] X.-Z. Liu, Z. Ye, Y. Dong, P. Egberts, R. W. Carpick, and A. Martini, *Phys. Rev. Lett.* **114**, 146102 (2015).
- [19] J. Nakamura, S. Wakunami, and A. Natori, *Phys. Rev. B* **72**, 235415 (2005).
- [20] Z. Tshiprut, S. Zelner, and M. Urbakh, *Phys. Rev. Lett.* **102**, 136102 (2009).
- [21] Y. Dong, D. Perez, A. F. Voter, and A. Martini, *Tribol. Lett.* **42**, 99 (2011).
- [22] M. Evstigneev and P. Reimann, *Phys. Rev. B* **87**, 205441 (2013).
- [23] C. M. Mate, G. M. McClelland, R. Erlandsson, and S. Chiang, *Phys. Rev. Lett.* **59**, 1942 (1987).
- [24] S. N. Medyanik, W. K. Liu, I.-H. Sung, and R. W. Carpick, *Phys. Rev. Lett.* **97**, 136106 (2006).
- [25] R. Roth, T. Glatzel, P. Steiner, E. Gnecco, A. Baratoff, and E. Meyer, *Tribol. Lett.* **39**, 63 (2010).
- [26] A. Benassi, A. Vanossi, and E. Tosatti, *Nat. Commun.* **2**, 236 (2011).
- [27] D. Mandelli, A. Vanossi, and E. Tosatti, *Phys. Rev. B* **87**, 195418 (2013).
- [28] I. García-Mata, O. V. Zhironov, and D. L. Shepelyansky, *Eur. Phys. J. .direct D* **41**, 325 (2007).
- [29] T. Pruttivarasin, M. Ramm, I. Talukdar, A. Kreuter, and H. Häffner, *New J. Phys.* **13**, 075012 (2011).
- [30] D. Gangloff, A. Bylinskii, I. Counts, W. Jhe, and V. Vuletić, *Nat. Phys.* **11**, 915 (2015).
- [31] A. Bylinskii, D. Gangloff, and V. Vuletić, *Science* **348**, 1115 (2015).
- [32] A. Bylinskii, D. Gangloff, I. Counts, and V. Vuletić, *Nat. Mater.* **15**, 717 (2016).
- [33] M. Enderlein, T. Huber, C. Schneider, and T. Schaetz, *Phys. Rev. Lett.* **109**, 233004 (2012).
- [34] R. B. Linnet, I. D. Leroux, M. Marciante, A. Dantan, and M. Drewsen, *Phys. Rev. Lett.* **109**, 233005 (2012).
- [35] L. Karpa, A. Bylinskii, D. Gangloff, M. Cetina, and V. Vuletić, *Phys. Rev. Lett.* **111**, 163002 (2013).
- [36] K. Shinjo and M. Hirano, *Surf. Sci.* **283**, 473 (1993).
- [37] M. Hirano, K. Shinjo, R. Kaneko, and Y. Murata, *Phys. Rev. Lett.* **78**, 1448 (1997).
- [38] M. Dienwiebel, G. S. Verhoeven, N. Pradeep, J. W. M. Frenken, J. A. Heimberg, and H. W. Zandbergen, *Phys. Rev. Lett.* **92**, 126101 (2004).
- [39] A. Socoliuc, R. Bennewitz, E. Gnecco, and E. Meyer, *Phys. Rev. Lett.* **92**, 134301 (2004).
- [40] J. Kiethe, R. Nigmatullin, D. Kalincev, T. Schmirander, and T. E. Mehlstaubler, *Nat. Commun.* **8**, 15364 (2017).
- [41] M. Cetina, A. Bylinskii, L. Karpa, D. Gangloff, K. M. Beck, Y. Ge, M. Scholz, A. T. Grier, I. Chuang, and V. Vuletić, *New J. Phys.* **15**, 053001 (2013).
- [42] L. Prandtl, *Z. Angew. Math. Mech.* **8**, 85 (1928).
- [43] G. A. Tomlinson, *Philos. Mag.* **7**, 905 (1929).
- [44] See Supplemental Material at <http://link.aps.org/supplemental/10.1103/PhysRevLett.119.043601> for a derivation of equations used in the text and an elaboration of the data analysis.
- [45] K. B. Jinesh, S. Y. Krylov, H. Valk, M. Dienwiebel, and J. W. M. Frenken, *Phys. Rev. B* **78**, 155440 (2008).
- [46] Y. Sang, M. Dubé, and M. Grant, *Phys. Rev. Lett.* **87**, 174301 (2001).